AIP | Applied Physics Letters

Three-dimensional control of Tetrahymena pyriformis using artificial magnetotaxis

Dal Hyung Kim, Paul Seung Soo Kim, Anak Agung Julius, and Min Jun Kim

Citation: Appl. Phys. Lett. **100**, 053702 (2012); doi: 10.1063/1.3678340
View online: http://dx.doi.org/10.1063/1.3678340
View Table of Contents: http://apl.aip.org/resource/1/APPLAB/v100/i5
Published by the American Institute of Physics.

Three-dimensional control of *Tetrahymena pyriformis* using artificial magnetotaxis

Dal Hyung Kim,[1] Paul Seung Soo Kim,[1] Anak Agung Julius,[2] and Min Jun Kim[1,a)]
[1]*Department of Mechanical Engineering & Mechanics, Drexel University, Philadelphia, Pennsylvania 19104, USA*
[2]*Department of Electrical, Computer and Systems Engineering, Rensselaer Polytechnic Institute, Troy, New York 12180, USA*

(Received 19 November 2011; accepted 2 January 2012; published online 2 February 2012)

We demonstrate three-dimensional control with the eukaryotic cell *Tetrahymena pyriformis* (*T. pyriformis*) using two sets of Helmholtz coils for *xy*-plane motion and a single electromagnet for *z*-direction motion. *T. pyriformis* is modified to have artificial magnetotaxis with internalized magnetite. To track the cell's z-axis position, intensity profiles of non-motile cells at varying distances from the focal plane are used. During vertical motion along the *z*-axis, the intensity difference is used to determine the position of the cell. The three-dimensional control of the live microorganism *T. pyriformis* as a cellular robot shows great potential for practical applications in microscale tasks, such as target transport and cell therapy. © *2012 American Institute of Physics*. [doi:10.1063/1.3678340]

Developing microrobots for low Reynolds number environment entails developing swimming systems that can overcome viscous forces. Swimming mechanisms found in nature have elegant solutions to this problem, such as flagella and cilia used by microorganisms. Researchers have already investigated means to imitate or harness these motile organelles for use in microrobotics.[1–6] Recently, we successfully harnessed *Tetrahymena pyriformis* (*T. pyriformis*) as microrobots. Through magnetite internalization by the cells, we were able to fully control *T. pyriformis* using a magnetic field[7] and then track them in two dimensions.[8] In this paper, three-dimensional (3D) control of artificial *T. pyriformis* is accomplished through the use of a multifunctional approximate Helmholtz coil system. To track the cell's position in the *z*-axis, intensity profiles of deciliated cells are obtained at different depths. We used an open loop control system to steer *T. pyriformis* and then used the predetermined intensity profile to calculate the cell's trajectory.

T. pyriformis is cultured in culture medium with 0.1% (w/v) select yeast extract (Sigma Aldrich, MO, USA) and 1% (w/v) tryptone (Sigma Aldrich) in deionized water. Cell cultures are maintained at 28 °C in an incubator.[9] Figure 1(a) shows that the average cell size of *T. pyriformis* is 25 μm by 50 μm. Its entire cell body is covered with approximately 600 cilia, consisting of both motile and oral cilia.[10] Artificial magnetotactic *T. pyriformis*, Figure 1(b), is obtained by allowing *T. pyriformis* cells to ingest and internalize iron oxide particles.[7]

For our system, two sets of approximate Helmholtz coils are used for *x* and *y* axes control, and one electromagnetic coil is utilized for *z*-axis control. The coil frame is set on an inverted microscope (Leica DM IRB) and the images are captured at 10 frames per second using a camera (MotionPro X3). An image processing algorithm calculates the positions of the cells using the captured images. In Figure 1(c), both the top and bottom of the coil configuration are illustrated. The approximate Helmholtz coils are designed to generate uniform magnetic fields of about 2.5 mT to exert a torque without translational force. The *xy*-direction of the magnetic fields exerted is controlled using the combination of the *x* and *y* sets of Helmholtz coils. The one *z*-axis electromagnet is located on the bottom of the stage and placed close to the sample in order to expose the cells to a stronger magnetic field and steer them in the *z*-direction.

The gradient of the magnetic fields is negligible in the working space from −3 mm to 3 mm when only one set of Helmholtz coils is activated. Since there is a negligible gradient in the experiment field of view, we assumed only torque is exerted along the *x* and *y* axis. Figure 1(e) shows the simulation results at the center ($(x, y) = (0, 0)$) when only one coil in z-axis is activated. The magnetic fields along the *z*-direction exhibited a strength of about 5.5 mT with relative uniformity at the center, while the *x* and *y* components of the fields are small enough to be negligible. Hence, the electromagnetic coil system has the capability to manipulate magnetic fields in *xyz*-direction with precise specifications, allowing for the control of artificial magnetotactic *T. pyriformis* in 3D.

The major challenge of microscale 3D tracking is that only the focal plane is available for observation when using the microscope in most cases. 3D tracking of microspheres has been widely studied and well established because their *z*-axis position may be accurately calculated with its Gaussian distributed intensity profile.[11] However, 3D tracking of microorganisms and determination of their *z*-axis position are difficult due to the deformation and uneven intensity profile of a cell. The shape of *T. pyriformis* cells is not perfectly spherical and their intensity profile is different from a Gaussian distribution because the intensity inside of the cell is similar with the background while that of the membrane differs. When a cell is far from the focal plane, the image is blurred, resulting in a decrease of the maximum intensity and a widening of the intensity distribution.

a)Electronic mail: mkim@coe.drexel.edu.

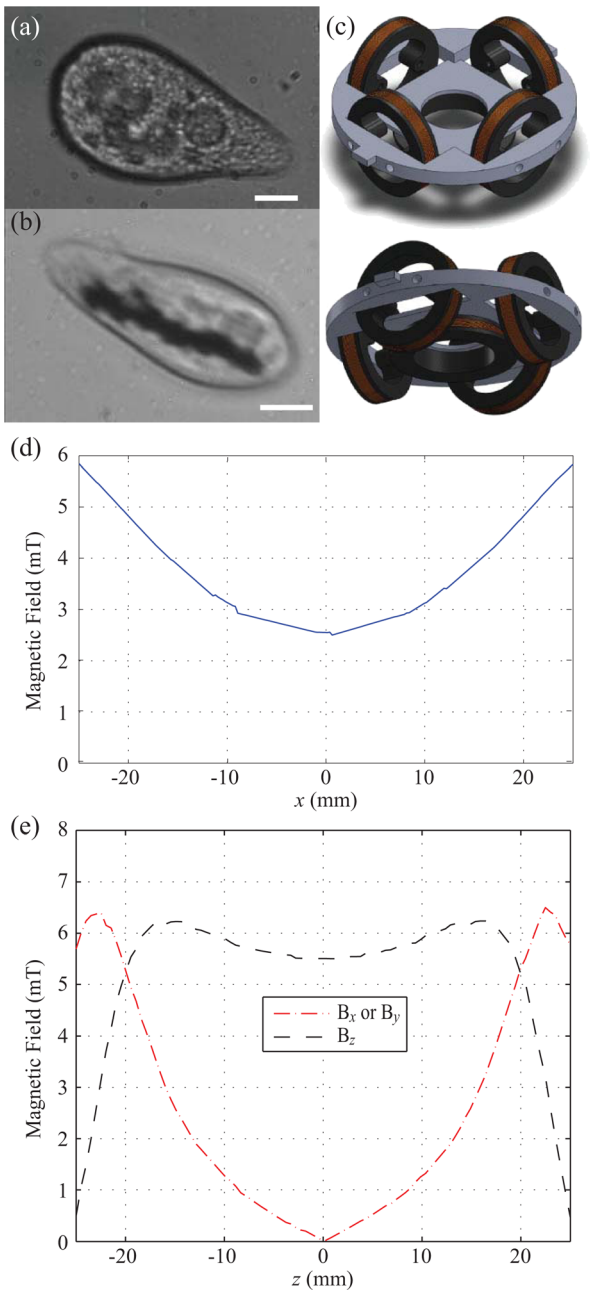

FIG. 1. (Color online) (a) Normal *T. pyriformis* cell and (b) with ingested magnetite. The scale bar is 10 μm. (c) Coil configuration drawing in two different views. (d)-(e) Simulation result of the strength of the magnetic fields (d) when only one set of Helmholtz coils in *x*-axis and (e) only one coil in *z*-axis are activated, respectively.

The intensity information of the cell is used to estimate the *z*-axis position. The intensity difference between cells and the background is quite consistent; therefore, a mean intensity difference is used in this experiment. The intensity of the cell is determined by the average intensity of the pixels occupied by the cell, while that of the background is determined by the immediate unoccupied area around the cell. To understand the relationship between the mean intensity difference and a cell's position in *z*-axis, non-motile *T. pyriformis* were prepared and observed under the microscope while changing the focal plane. Non-motile *T. pyriformis* was obtained through a deciliation process.[12,13] Further observation revealed that deciliated cells have similar intensity profiles as their ciliated counterparts.

Figure 2 shows the mean intensity difference between a cell and the background versus the *z*-axis position. Ten cells have been observed from 0 to 500 μm in the *z*-axis, where 0 μm is defined as a cell in focus, and a positive value denotes an increase in distance between the original focal plane (0 μm) and the objective. The circle and cross markers represent the first region from 0 to 20 μm and the second region represents the next increment of 20 μm, where each marker represents a captured image of the cell; there are about 300 markers total. From 0 to 20 μm in the *z*-axis, the mean intensity difference increases; beyond 20 μm, it decreases exponentially. Thus, curve fitting was separately conducted for each region. One data set from 0 to 20 μm in the *z*-axis was fitted with the linear curve, whose slope is 1.375 μm^{-1}. The other data set from 20 to 500 μm in the *z*-axis was fitted with the exponential equation expressed in Eq. (1).

$$I = ae^{-bz} + c, \tag{1}$$

where I is the mean intensity difference and z is the position in *z*-axis. The parameters a, b, and c are 75.13, 0.004, and 7.316, respectively. When the position in the *z*-axis is 20 μm, the mean intensity difference has a maximum value of 76.51. *T. pyriformis* normally swim above the substrate, so we assumed that the cell swims 20 μm above the substrate which is focused as a datum. The position in *z*-axis is estimated by Eq. (1).

The cell's 3D motion was controlled in two different modes: planar (*xy*-plane motion) and vertical (*z*-axis motion). Planar motion is controlled using the two sets of Helmholtz coils while vertical motion is controlled using only the single *z*-axis coil. Figures 3(a)–3(l) show the sequence of images of the manually controlled *T. pyriformis* where the lines and circle markers represent the trajectories and centroids, respectively. The cell's trajectory can be seen in Figure 3(m), where the planar mode of motion can occurs in two distinct *xy*-planes. The *xy*-planes that are about 127.0 μm and

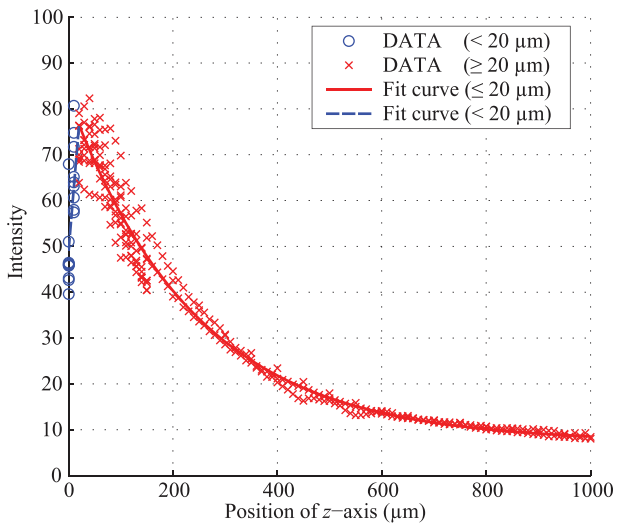

FIG. 2. (Color online) The intensity difference of *T. pyriformis* from that of the background from 0 to 500 μm. From 0 to 20 μm, the intensity difference increases and the data are fitted with a linear curve. From 20 to 500 μm, it decreases exponentially and the data are fitted using Eq. (1).

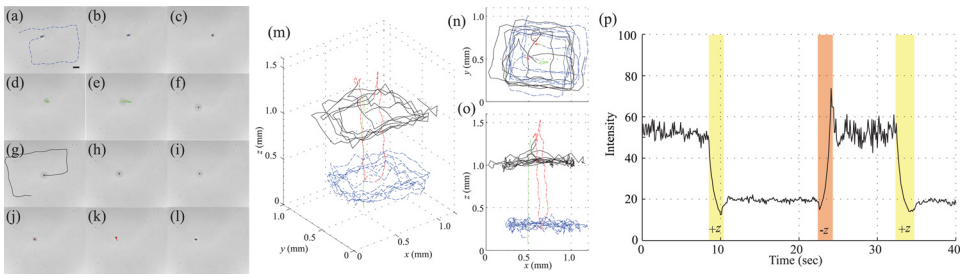

FIG. 3. (Color online) The manual control experiment. (a)-(l) The sequence of images of (a) planar motion at around 127.0 μm from the focal plane, (b)-(f) upward vertical motion, (g) planar motion at around 446.6 μm from the focal plane, and (h)-(l) downward vertical motion. The scale bar is 100 μm. (m) The trajectory in a 3D view, (n) a view of *xy*-plane, and (o) *xz*-plane. The dashed and solid lines represent the trajectories in the lower plane and the upper plane, respectively. The dashed-dot and dotted lines represent the trajectories in the *z*-axis for upwards and downwards motion, respectively. (p) The intensity difference of the tracked cell. Light and dark yellow regions represent the period when positive and negative magnetic fields are applied along the *z*-axis, respectively.

446.6 m above the focal plane can be referred to as the lower plane and upper place, respectively. Fluctuations observed in both modes are due to the corkscrew motion of the cells.

In Figure 3(a), *T. pyriformis* was controlled in planar mode in the lower plane. Figures 3(b)–3(f) are the series of pictures when the cell swims from the lower to the upper plane. Figures 3(d) and 3(e) show the cell and its trajectory when it moves along the *z*-axis. When the cell moves upward, the difference between the cell's intensity and the background decreased. In Figure 3(f), the cell's motion was switched to planar mode in the upper plane. In Figure 3(g), the upper plane trajectory can be observed where the cell appears to be an amorphous blur. The intensity difference of the cell between the background is still recognizable but difficult to distinguish. From Figures 3(h)–3(k), downward movement in the *z*-axis is illustrated. Figures 3(h) and 3(i) are the images before and after vertical mode is engaged, respectively. Since the cell is located far from the focal plane, it is hard to observe the change of its shape, as observed in Figures 3(b) and 3(c). The downward helical swimming is illustrated in Figures 3(i)–3(k). As the cell moves closer to the focal plane, it becomes distinct from the background and their intensity difference increased. Figure 3(l) shows the motion in the lower plane after travelling along the *z*-axis. The original pear-shape of the cell is observed because it is close to the focal plane. The entire 3D, *xy*-plane, and *xz*-plane trajectories are illustrated in Figures 3(m)–3(o), respectively.

The intensity difference during the experiment is shown in Figure 3(p). The intensity difference between the cell and the background is greater when the cell is focused. In contrast, the intensity difference decreases when the cell moves away from the focal plane. From 0 to 8.5 s and 24.7 to 32.3 s, the cell travelled on the lower plane. Thus, the intensity difference is high. Since the cell is controlled in the upper plane between 10.7 and 22.3 s and after 34.8 s, the intensity difference is low. The fluctuation of the intensity difference when the cell moves in the lower plane is higher than that of the upper plane, while the variance of the *z*-axis position for both cases are similar at 19.0 and 19.4 μm for the lower and upper plane, respectively. Also, during planar mode, its fluctuation in the *z*-axis is also about 38 μm. This fluctuation is due to the small position difference in the *z*-axis around the focal plane, creating a large intensity difference based on the graph in Figure 2, which decreases exponentially.

In this paper, we have demonstrated 3D control of a live organism, artificial magnetotactic *T. pyriformis*, as a microrobot and tracked its 3D position using the intensity information of the cell. Artificial magnetotactic *T. pyriformis*, which internalizes iron oxide particles, was controlled by manipulating the swimming direction of a cell in 3D space using two sets of Helmholtz coils and one coil for the z-axis. The locations in the *z*-axis were evaluated using the mean intensity of a cell which decreased exponentially above 20 μm from the focal plane.

This work was funded by NSF CMMI Control Systems (Award No. 1000284) and CBET Fluid Dynamics (Award No. 0828167).

[1]L. Zhang, K. E. Peyer, and B. J. Nelson, Lab Chip **10**(17), 2203 (2010).
[2]A. Ghosh and P. Fischer, Nano Lett. **9**(6), 2243 (2009).
[3]L. Zhang, J. J. Abbott, L. Dong, B. E. Kratochvil, D. Bell, and B. J. Nelson, Appl. Phys. Lett. **94**(6), 064107 (2009).
[4]L. Zhang, J. J. Abbott, D. Lixin, B. E. Kratochvil, Z. Haixin, K. E. Peyer, and B. J. Nelson, in Intelligent Robots and Systems, 2009. IROS 2009. IEEE/RSJ International Conference (IEEE, 2009), pp. 1401–1406, DOI: 10.1109/IROS.2009.5354314.
[5]U. K. Cheang, D. Roy, J. H. Lee, and M. J. Kim, Appl. Phys. Lett. **97**, 213704 (2010).
[6]S. Martel, Int. J. Adv. Syst. Meas. **3**(3 and 4), 92 (2011).
[7]D. H. Kim, U. K. Cheang, L. Kőhidai, D. Byun, and M. J. Kim, Appl. Phys. Lett. **97**(17), 173702 (2010).
[8]D. H. Kim, S. Brigandi, A. A. Julius, and M. J. Kim, in *Robotics and Automation* (ICRA), 2011 IEEE International Conference, Shanghai, China (IEEE, 2011), pp. 3183–3188, DOI: 10.1109/ICRA.2011.5980107.
[9]L. Kőhidai and G. Csaba, Comp. Biochem. Physiol., Part C: Pharmacol., Toxicol. Endocrinol. **111**(2), 311 (1995).
[10]D. H. Kim, D. Casale, L. Kőhidai, and M. J. Kim, Appl. Phys. Lett. **94**(16), 163901 (2009).
[11]C. Cierpka, M. Rossi, R. Segura, and C. Kähler, Meas. Sci. Technol. **22**, 015401 (2011).
[12]D. H. Kim, S. E. Brigandi, P. Kim, D. Byun, and M. J. Kim, J. Bionic Eng. **8**(3), 273 (2011).
[13]G. A. Thompson, Jr., L. C. Baugh, and L. F. Walker, J. Cell Biol. **61**(1), 253 (1974).